



Sulfur dioxide (SO₂) as observed by MIPAS/Envisat: temporal development and spatial distribution at 15–45 km altitude

M. Höpfner¹, N. Glatthor¹, U. Grabowski¹, S. Kellmann¹, M. Kiefer¹, A. Linden¹, J. Orphal¹, G. Stiller¹, T. von Clarmann¹, B. Funke², and C. D. Boone³

¹Institute for Meteorology and Climate Research, Karlsruhe Institute of Technology, Karlsruhe, Germany

²Instituto de Astrofísica de Andalucía, CSIC, Granada, Spain

³Department of Chemistry, University of Waterloo, Waterloo, Ontario, Canada

Correspondence to: M. Höpfner (michael.hoepfner@kit.edu)

Received: 29 March 2013 – Published in Atmos. Chem. Phys. Discuss.: 14 May 2013

Revised: 16 August 2013 – Accepted: 19 September 2013 – Published: 29 October 2013

Abstract. We present a climatology of monthly and 10° zonal mean profiles of sulfur dioxide (SO₂) volume mixing ratios (vmr) derived from MIPAS/Envisat measurements in the altitude range 15–45 km from July 2002 until April 2012. The vertical resolution varies from 3.5–4 km in the lower stratosphere up to 6–10 km at the upper end of the profiles, with estimated total errors of 5–20 pptv for single profiles of SO₂. Comparisons with the few available observations of SO₂ up to high altitudes from ATMOS for a volcanically perturbed situation from ACE-FTS and, at the lowest altitudes, with stratospheric in situ observations reveal general consistency of the datasets. The observations are the first empirical confirmation of features of the stratospheric SO₂ distribution, which have only been shown by models up to now: (1) the local maximum of SO₂ at around 25–30 km altitude, which is explained by the conversion of carbonyl sulfide (COS) as the precursor of the Junge layer; and (2) the downwelling of SO₂-rich air to altitudes of 25–30 km at high latitudes during winter and its subsequent depletion on availability of sunlight. This has been proposed as the reason for the sudden appearance of enhanced concentrations of condensation nuclei during Arctic and Antarctic spring. Further, the strong increase of SO₂ to values of 80–100 pptv in the upper stratosphere through photolysis of H₂SO₄ has been confirmed. Lower stratospheric variability of SO₂ could mainly be explained by volcanic activity, and no hints of a strong anthropogenic influence have been found. Regression analysis revealed a QBO (quasi-biennial oscillation) signal of the SO₂ time series in the tropics at about 30–35 km, an SAO (semi-annual oscillation) signal at tropical and subtropical

latitudes above 32 km and annual periodics predominantly at high latitudes. Further, the analysis indicates a correlation with the solar cycle in the tropics and southern subtropics above 30 km. Significant negative linear trends are found in the tropical lower stratosphere, probably due to reduced tropical volcanic activity and at southern mid-latitudes above 35 km. A positive trend is visible in the lower and middle stratosphere at polar to subtropical southern latitudes.

1 Introduction

Sulfur dioxide (SO₂) is one of the key species determining the aerosol content of the stratosphere (SPARC, 2006). Main sources of stratospheric SO₂ are the conversion of carbonyl sulfide (COS) (Crutzen, 1976; Brühl et al., 2012) and the direct transport of SO₂ across the tropopause. This transport can occur abruptly through major volcanic eruptions, through upwelling predominantly at the tropical tropopause or through the monsoon circulation (Bourassa et al., 2012). However, there is still a lot of uncertainty regarding the major sources of stratospheric SO₂ during volcanically quiescent periods (Deshler et al., 2006; Hofmann et al., 2009; Vernier et al., 2011; Solomon et al., 2011; Brühl et al., 2012).

Loss of SO₂ occurs mainly through oxidation by OH radicals into H₂SO₄ vapour, which condenses into liquid sulfate aerosols. Subsequently, sedimentation of particles results in a loss of sulfur from the stratosphere. Large-scale circulation leads to further upwelling of sulfur species in the tropical stratosphere, where the photolysis of H₂SO₄ constitutes

a probable further source of SO₂ (Rinsland et al., 1995; Vaida et al., 2003; Mills et al., 2005). During winter, downwelling of air in the polar vortices transports elevated amounts of SO₂ from the upper stratosphere down to altitudes of 30 km and below. Here, on availability of sunlight in spring, SO₂ is transformed through reaction with OH into H₂SO₄, thus leading to the formation of new particles. These processes have been proposed by Zhao et al. (1995) and Mills et al. (1999, 2005) as an explanation for the sudden formation of enhanced layers of condensation nuclei (CN) in polar spring (Rosen and Hofmann, 1983; Hofmann and Rosen, 1985; Hofmann, 1990; Wilson et al., 1990). However, there has been no direct experimental evidence for this mechanism until now.

There exists a large dataset of SO₂ observations from spaceborne nadir-sounding instruments (e.g. Theys et al., 2012, and references therein). While these measurements have a good horizontal resolution, height-resolved profiles cannot be obtained (although some information on plume height has recently been derived: Van Gent et al., 2012; Carboni et al., 2012). Hence, measurements of the vertical distribution of SO₂ in the stratosphere are sparse. This is, for example, reflected in one of the recommendations within SPARC (2006, p. xii): “Observations of SO₂ in the upper troposphere and lower stratosphere and of H₂SO₄ and SO₂ in the middle and upper stratosphere would be extremely valuable to improve our modelling and predictive capabilities of stratospheric aerosol.” Under volcanically perturbed situations enhanced mixing ratios of SO₂ facilitate their measurement. For example, the SO₂ cloud from the eruption of Mt Pinatubo in June 1991 was analysed on the basis of UARS-MLS observations by Read et al. (1993), and ACE-FTS measurements were used to investigate SO₂ and sulfate aerosol from the Sarychev eruption in June 2009 (Doeringer et al., 2012).

Only three measured profiles of SO₂ covering the altitude range of the stratosphere have been published so far (Rinsland et al., 1995). In their work, on the basis of mean infrared solar occultation spectra during three spaceborne flights of the ATMOS instrument, one SO₂ vertical profile per flight was derived for the altitude range of about 30–50 km. The data revealed high concentrations of SO₂ in the upper stratosphere in the range 100–400 pptv, which was explained by photolysis of H₂SO₄. However, two of those profiles were strongly perturbed by the Pinatubo eruption and one possibly, but to a much lesser extent, by El Chichón. Thus, there exists at most one observation of the background stratospheric SO₂ distribution.

In the present work we have analysed infrared limb-emission measurements by MIPAS/Envisat to obtain a global climatology of stratospheric SO₂ distributions from July 2002 until April 2012. First attempts at the retrieval of SO₂ from MIPAS have previously been performed by Burgess et al. (2005).

After an overview of the instrument (Sect. 2), the retrieval strategy and data characterisation will be described (Sect. 3). Then an overview of the dataset will be given in Sect. 4, followed by an assessment of its quality through comparison with independent observations and analysis of the internal variability (Sect. 5). In Sect. 6 the distribution of SO₂ will be discussed with respect to the various processes described above, including a regression analysis to single out correlations with external parameters, periodic cycles and trends.

2 Instrument

MIPAS (Michelson Interferometer for Passive Atmospheric Sounding) is one of the instruments on ESA's polar orbiting Envisat satellite (Fischer et al., 2008). Envisat was launched on 1 March 2002, and remained in operation until 8 April 2012, when contact was lost. With one major interruption from April to December 2004, MIPAS measured quasi-continuously from July 2002 until April 2012. The MIPAS FTIR (Fourier transform infrared) limb sounder recorded the radiation emitted by the Earth's atmosphere in the mid-infrared region with a spectral resolution of 0.025 cm⁻¹ before April 2004 (period 1, P1) and 0.0625 cm⁻¹ from January 2005 onwards (period 2, P2). MIPAS was periodically operated in different limb scan patterns. For this work we have used the most frequent “nominal” viewing modes. During P1 these consisted of 17 tangent altitudes (6–68 km with 3 km distances up to 42 km, followed by two steps of 5 km and two steps of 8 km), which do not depend on the geographical position. During P2 the number of tangent views per limb scan was increased to 27. Here tangent altitudes depend on latitude ranging from 5–70 km at the poles to 12–77 km over the Equator, with steps increasing with height from 1.5 to 4.5 km. The horizontal distance between two subsequent limb scans in nominal measurement mode was around 550 km during P1 and 420 km during P2, resulting in about 1000 and 1400 limb scans providing full latitudinal coverage per day.

3 Retrieval

Retrieval of SO₂ altitude profiles up to the middle stratosphere from MIPAS observations is difficult due to its small spectral signal relative to the spectral noise of MIPAS, especially under volcanically non-perturbed conditions. Therefore, we have chosen to analyse monthly mean limb spectra binned within 10°-wide latitude bands. This method has already been employed for the detection of stratospheric BrONO₂ in Höpfner et al. (2009a).

In detail, first cloud clearing has been performed on the basis of the cloud-index (CI) method (Spang et al., 2004). This is necessary to avoid retrieval errors due to cloud/aerosol signal in the spectra. The CI is the spectral radiance contrast between two wavenumbers. A smaller CI indicates larger probability that the spectrum is contaminated by aerosols or

clouds. We use a CI threshold of 4.5; that is, spectra with $CI < 4.5$ are discarded. Further, all spectra in this limb sequence are discarded which were measured at lower tangent altitudes than those with $CI < 4.5$. Beside thick tropospheric clouds, this approach excludes, for example, also cirrus clouds, polar stratospheric clouds (Höpfner et al., 2009b) and optically thicker aerosol plumes from the subsequent analysis. Depending on atmospheric situation, particle composition and altitude, the applied CI limit equals a particle volume density of about $1\text{--}2\ \mu\text{m}^3\ \text{cm}^{-3}$.

In the second step the limb scans that are averaged within each latitude- and time bin are selected. Here we have chosen those locations with the lowest available tangent altitude after cloud clearing under the condition that at least 300 limb scans are averaged, which reduced the noise by a factor of at least 17. The noise reduction could be further improved by increasing the required number of samples; this, however, would lead to loss of measurement points particularly at low altitudes and during months with sparser observational coverage. A decrease of the required number of samples, on the other hand, would result in larger noise error contributions. For this analysis, MIPAS version 5 level-1b data have been used. Together with the averaged MIPAS spectra, for the retrieval mean, pressure–temperature profiles are calculated from ECMWF analysis data at the position of each single limb scan. Further, mean tangent altitudes are obtained from the engineering MIPAS tangent altitude values. Errors resulting from these averaging processes are included in the error estimation as described further below.

The retrieval scheme is a constrained global fit approach using all tangent altitudes of one limb scan with averaged spectra simultaneously (e.g. von Clarmann et al., 2003a):

$$\mathbf{x}_{i+1} = \mathbf{x}_i + \left(\mathbf{K}_i^T \mathbf{S}_y^{-1} \mathbf{K}_i + \mathbf{R} \right)^{-1} \times \left[\mathbf{K}_i^T \mathbf{S}_y^{-1} (\mathbf{y}_{\text{meas}} - \mathbf{y}(\mathbf{x}_i)) - \mathbf{R}(\mathbf{x}_i - \mathbf{x}_a) \right], \quad (1)$$

which is a variant of the formulation suggested by Rodgers (2000). Here, \mathbf{x} is the vector containing the atmospheric and instrumental parameters to be determined. The atmospheric profiles are gridded at 1 km altitude levels reaching from 0 to 100 km, in between which the volume mixing ratios (vmr) vary linearly with height. \mathbf{y}_{meas} are the averaged measured radiances of all tangent altitudes, and \mathbf{S}_y is the measurement noise covariance matrix. \mathbf{y}_i contains the spectral radiances, which are simulated with the radiative transfer model KOPRA (Stiller, 2000) using the results obtained in iteration number i . \mathbf{K}_i is the Jacobian matrix, i.e. the partial derivatives $\partial \mathbf{y}(\mathbf{x}_i) / \partial \mathbf{x}_i$ determined in parallel to \mathbf{y}_i at each iteration step. \mathbf{x}_a contains the a priori profiles. For the target species SO₂, altitude-independent initial guess and a priori profiles, \mathbf{x}_0 and \mathbf{x}_a equal 10 pptv, have been used, whereas for all other trace gases climatological values have been chosen.

For the regularisation matrix \mathbf{R} a first-order smoothing constraint $\mathbf{R} = \gamma \mathbf{L}^T \mathbf{L}$, where \mathbf{L} is a first-order finite-

differences operator (Tikhonov, 1963; Steck, 2002), has been used in order not to bias the retrieval results. Thus, the choice of the constant a priori value for SO₂ has no influence on the resulting profiles. The regularisation parameter γ depends only on the species and not on the altitude. It was chosen such to avoid instabilities showing up as oscillations in the retrieved atmospheric profiles.

Line-by-line calculations have been based on the HITRAN 2008 compilation including updates until 2010 (Rothman et al., 2009). The spectral intervals (microwindows) used for the retrieval are located in the same wavenumber region ($\sim 1366\text{--}1377\ \text{cm}^{-1}$) within the SO₂ ν_3 band as those selected for the analysis of ACE-FTS (Doeringer et al., 2012) and of ATMOS data (Rinsland et al., 1995). In detail, we have chosen the four microwindows $1366.575\text{--}1367.925\ \text{cm}^{-1}$, $1369.95\text{--}1370.375\ \text{cm}^{-1}$, $1371.2\text{--}1371.925\ \text{cm}^{-1}$ and $1376.0\text{--}1376.375\ \text{cm}^{-1}$ in the case of the high-spectral resolution mode of MIPAS (P1), and $1366.5625\text{--}1367.9375\ \text{cm}^{-1}$, $1369.9375\text{--}1370.375\ \text{cm}^{-1}$, $1371.1875\text{--}1371.9375\ \text{cm}^{-1}$ and $1376.0\text{--}1376.375\ \text{cm}^{-1}$ for the measurements during P2. These have been selected to gain a good sensitivity for SO₂ while avoiding the strongly interfering spectral signatures of other gases as much as possible. To further minimise these interferences the following gases have been jointly retrieved with SO₂: H₂O (isotopologues: H₂¹⁶O, HDO, H₂¹⁸O), CO₂, O₃, CH₄, HCN and HO₂. Further, instrumental parameters that have been included in the parameter vector \mathbf{x} are a spectral shift correction per microwindow and an additive calibration offset per microwindow and tangent altitude. No regularisation has been applied in the case of these instrumental quantities.

Figure 1 presents an example of the spectral fit achieved in all four microwindows for MIPAS measurements with higher (top three rows) and lower spectral resolution (bottom three rows). Spectral residuals between measurements and simulation are shown for the case where no SO₂ has been retrieved (second and fifth row) and under consideration of SO₂ (third and sixth row). It is obvious that in both cases, the fit residual is strongly improved by including SO₂ into the fit parameter vector, and that the residuals without SO₂ fit (black lines in second and fifth row) are mostly produced by SO₂ spectral signatures (green lines in second and fifth row).

For characterisation of the vertical resolution of the retrieval the related averaging kernels have been determined as

$$\mathbf{A} = \left(\mathbf{K}^T \mathbf{S}_y^{-1} \mathbf{K} + \mathbf{R} \right)^{-1} \mathbf{K}^T \mathbf{S}_y^{-1} \mathbf{K}. \quad (2)$$

The rows of \mathbf{A} represent the contributions of different altitudes to the retrieved vmr profile of SO₂, whereas the columns are the responses of the system to a delta function at the associated altitude. Typical averaging kernels are shown in Fig. 2 for period P1 (top) and P2 (bottom). The overall diagonal structures of \mathbf{A} demonstrate that the retrieval of SO₂ behaves well with better vertical resolution at

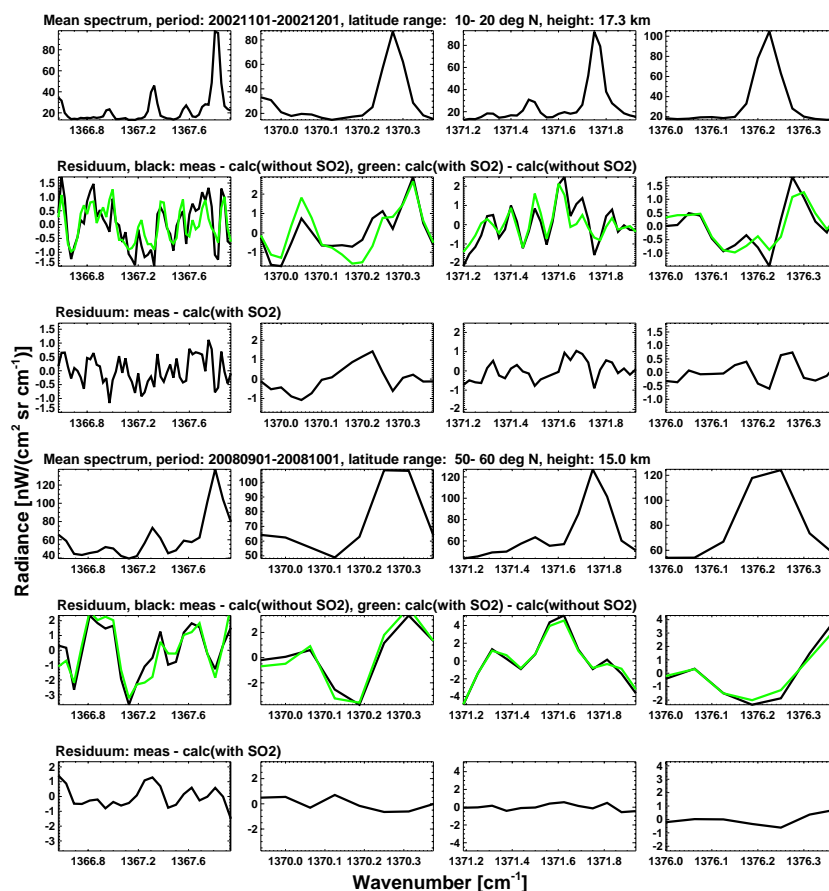


Fig. 1. Spectral identification and fit quality of the SO₂ retrieval. The columns show the four spectral windows used. The top three rows refer to the first observational period (P1), while rows 4–6 belong to the second period with lower spectral resolution (P2). Rows 1 and 4 contain the measured spectra. The black curves in the panels of row 2 and 5 show the residua after the spectral fit when no SO₂ is considered, and the black curves in row 3 and 6 are the residua in the case where SO₂ is added as a fitting parameter. The green curves in row 2 and 5 indicate the spectral features of SO₂ based on simulations only.

lower compared to higher altitudes due to the better sensitivity (higher pressure) and a denser tangent altitude sampling there. Typical values for the vertical resolution as derived from the width of the columns of **A** and from the inverse of the diagonal of **A** in both measurement modes vary around 3.5–4 km at 20 km, 4–5 km at 30 km and 6–10 km at 40 km altitude.

An estimate of the altitude dependent errors is presented in Fig. 3. Typical mean error profiles calculated for one month (January 2003) of period P1 and one month (January 2011) of P2 are shown together with the single error contributions which are combined into the total error by calculating the root sum squared of the single terms.

The following sources of uncertainty have been taken into account: spectroscopic errors of SO₂ line intensity (spe_int_SO₂) and air-broadened half-width (spe_hw_SO₂). For the line intensity an uncertainty of 5 % has been assumed, and for the half width one of 15 %. Both values are on the conservative side of the errors stated in Rothman et al.

(2009). The spectroscopy of interfering trace gas signatures has been handled as an independent error source by assigning also here errors of line intensity (spe_int_itf) and half-width (spe_hw_itf) of 5 % and 15 %, respectively. Major instrumental uncertainties are estimated as 1 % for gain calibration (gain), 3 % for the instrument line shape (ils) (in terms of linear loss of modulation efficiency toward the maximum optical path difference of the interferometer) and 300 m for tangent altitude pointing (htang). Spectral noise (noise) is based on the actual level 1b dataset as delivered together with the calibrated spectra. For the uncertainty of ECMWF temperatures (T_{ecm}), values of 2 K below and 5 K above 35 km altitude are assumed. A further error term that has to be taken into account for retrievals from averaged spectra is the effect of retrieval non-linearity (nlin). This error contribution is estimated on the basis of dedicated retrieval simulations as described in detail in Höpfner et al. (2009a) except that the values used for the line-of-sight uncertainty of single observations were 400 m for P1 and 300 m for the datasets during P2.

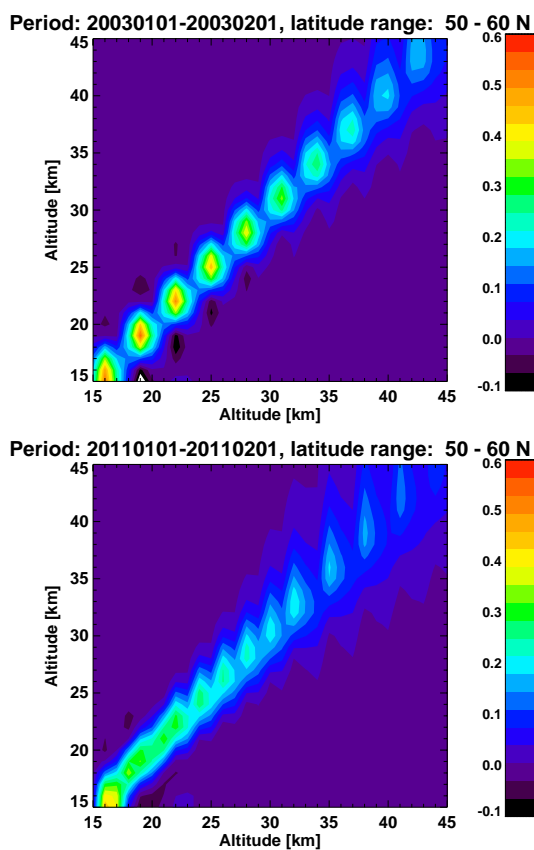


Fig. 2. Example of averaging kernels for SO₂ at mid-latitudes within the first (top) and the second (bottom) MIPAS measurement period.

These values have been determined from comparison of engineering tangent altitude values with those obtained by the pointing retrievals during the standard IMK/IAA data analysis (von Clarmann et al., 2003b, 2009; Kiefer et al., 2007).

4 Dataset overview

Figures 4–6 present an overview of all MIPAS results of SO₂ as colour-coded cross sections versus time. As mentioned above, the lower altitude limit of the dataset is defined by the condition on the minimum number of limb scans used to calculate mean spectra. This is determined by (a) the cloud coverage, (b) the scan pattern of MIPAS and (c) the lower limit of 15 km set to confine the retrievals mainly on the stratospheric situation. The influence of clouds can best be seen at the data gaps during the Antarctic winter season where the MIPAS observations are obscured by polar stratospheric clouds (e.g. top row in Fig. 4). High clouds also restrict some of the observations at low altitudes in tropical regions during P1 until March 2004. Further data gaps covering the whole altitude region are present in 2005 and 2006, when MIPAS

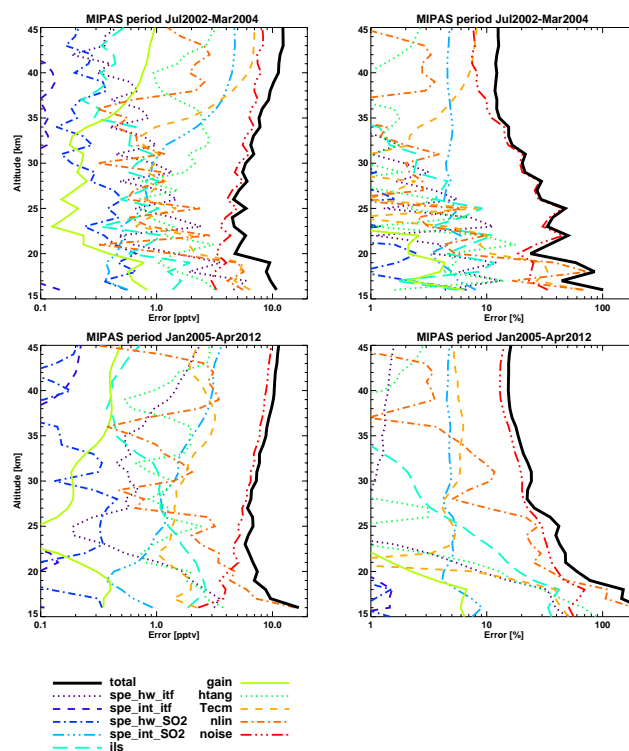


Fig. 3. Error estimation of the retrieval for one month during P1 and one month during P2. Considered error sources are the uncertainty of the foreign-broadened half-width and line intensity of interfering species (spe_hw_itf, spe_int_itf), the knowledge of these parameters for SO₂ (spe_hw_SO2, spe_int_SO2), the uncertainties of the instrumental line shape and gain calibration (ils, gain), the errors in the assumed tangent altitudes and temperatures (htang, Tecm), the error due to the applied technique of retrievals from averaged spectra (nlin) and the spectral noise of the instrument (noise). The total error has been determined by quadratic combination of the single error components.

measurements were still sparse during the first years in the new operational mode.

As a basis for subsequent discussions, the dataset has been reduced by averaging to the mean profiles for four seasons (see Fig. 7 and Fig. 8, top two rows). These profiles represent background situations since volcanically strongly perturbed periods, as detailed in the caption of Fig. 7, were neglected during averaging. The related variability is described in the bottom two rows of Fig. 8 by the altitude-dependent standard deviation.

5 Data quality

Here we assess the quality of the MIPAS SO₂ dataset by comparison with independent measurements. Furthermore, the estimation of random errors will be validated by comparison to the variability derived from the dataset itself.

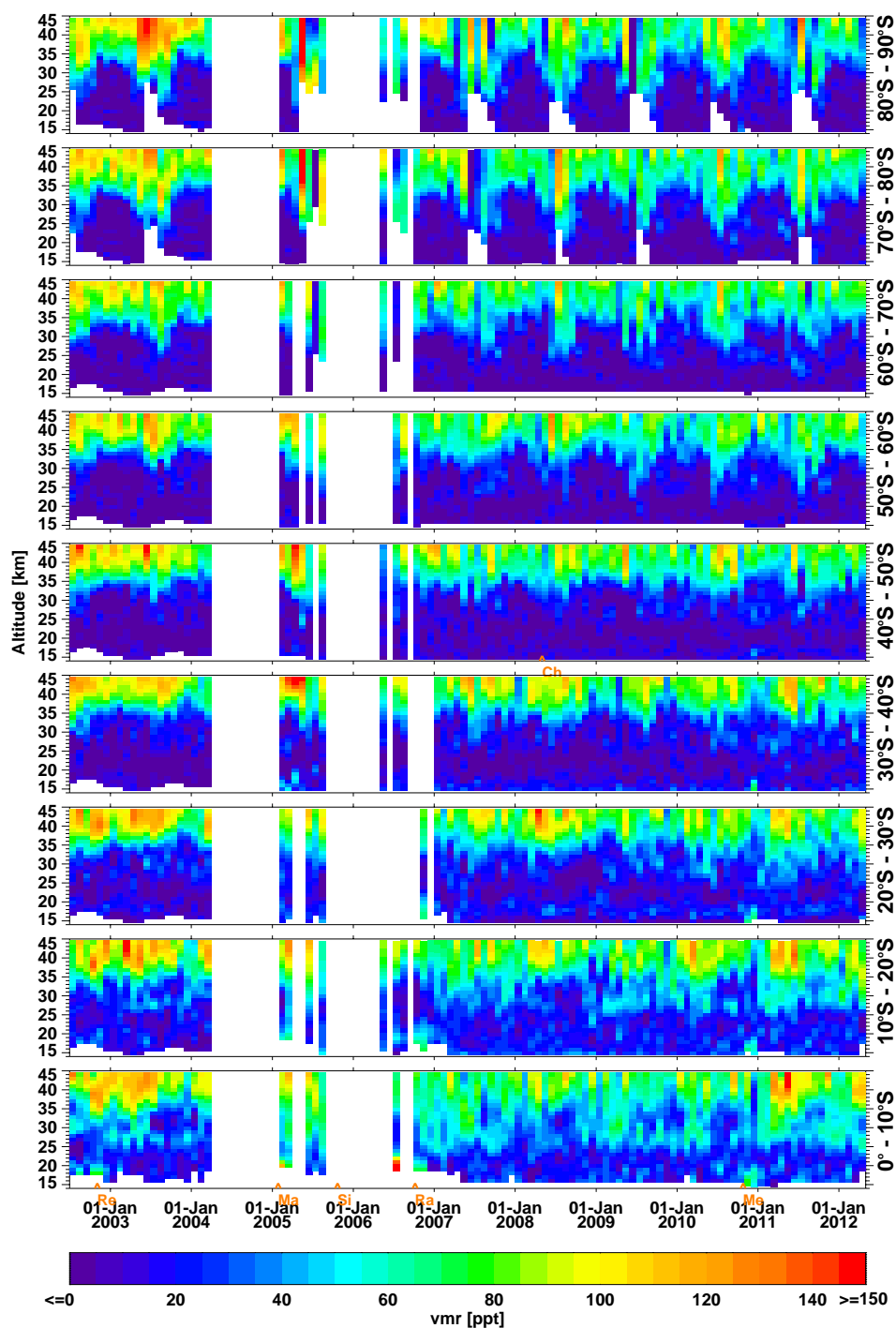


Fig. 4. Time series of colour-coded SO₂ monthly mean volume mixing ratio profiles for 10° latitude bins in the Southern Hemisphere. The colour scale is restricted to 0–150 pptv: negative values and those larger than 150 pptv are given the colour corresponding to 0 and 150 pptv, respectively. Major volcanic eruptions are indicated within the latitude bin of their location (see Table 2).

5.1 Comparison with ATMOS

The only measurements of SO₂ that have reached up to the upper stratosphere so far were published by Rinsland et al. (1995). These three profiles are compared with MIPAS data

obtained for similar latitudes and months in Fig. 9. The ATMOS profile of 1992 and, to a lesser extent, also that of 1993 are influenced by the eruption of Mt Pinatubo in June 1991 (Rinsland et al., 1995). Thus, the one that can best be compared to the MIPAS dataset is the ATMOS mean profile of

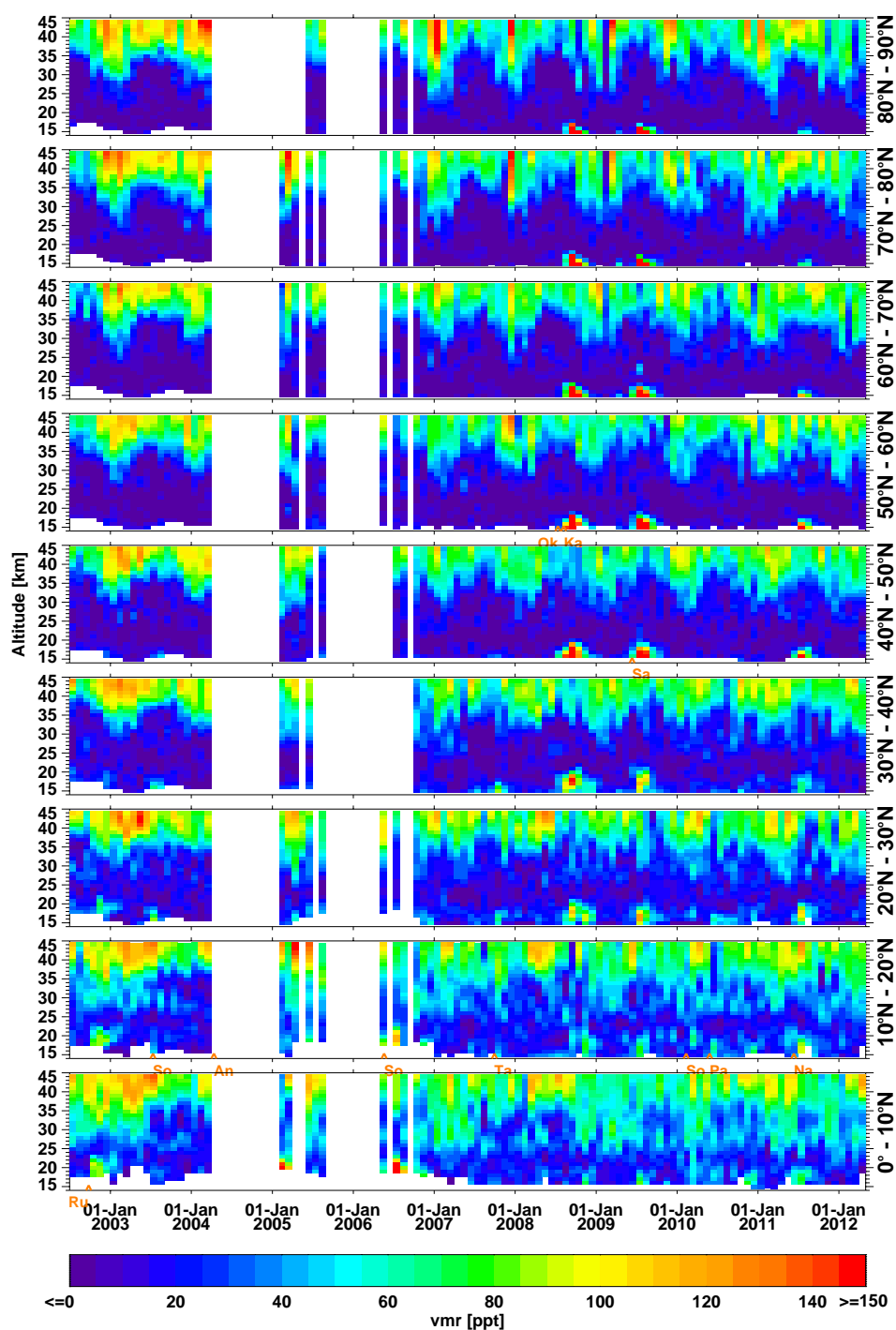


Fig. 5. Same as Fig. 4 but for the Northern Hemisphere.

1985. One should keep in mind that this has also been observed under enhanced stratospheric aerosol levels due to the eruption of El Chichón in March 1982, albeit to a lesser extent than ATMOS 1992 and 1993 (SPARC, 2006, e.g. Fig. 4.35).

Throughout the altitude range between 33 and 45 km, the MIPAS mean profile is within the uncertainty range of AT-

MOS 1985. Only at the lowest 2 km MIPAS mean volume mixing ratios of SO₂ are about 20 pptv larger than those of ATMOS. However, accounting for the variability, the MIPAS profiles are comparable to those of ATMOS at these altitudes. MIPAS agrees with both post-Pinatubo ATMOS measurements up to altitudes of 32 and 35 km, respectively. Above this, ATMOS shows strongly increasing concentrations up

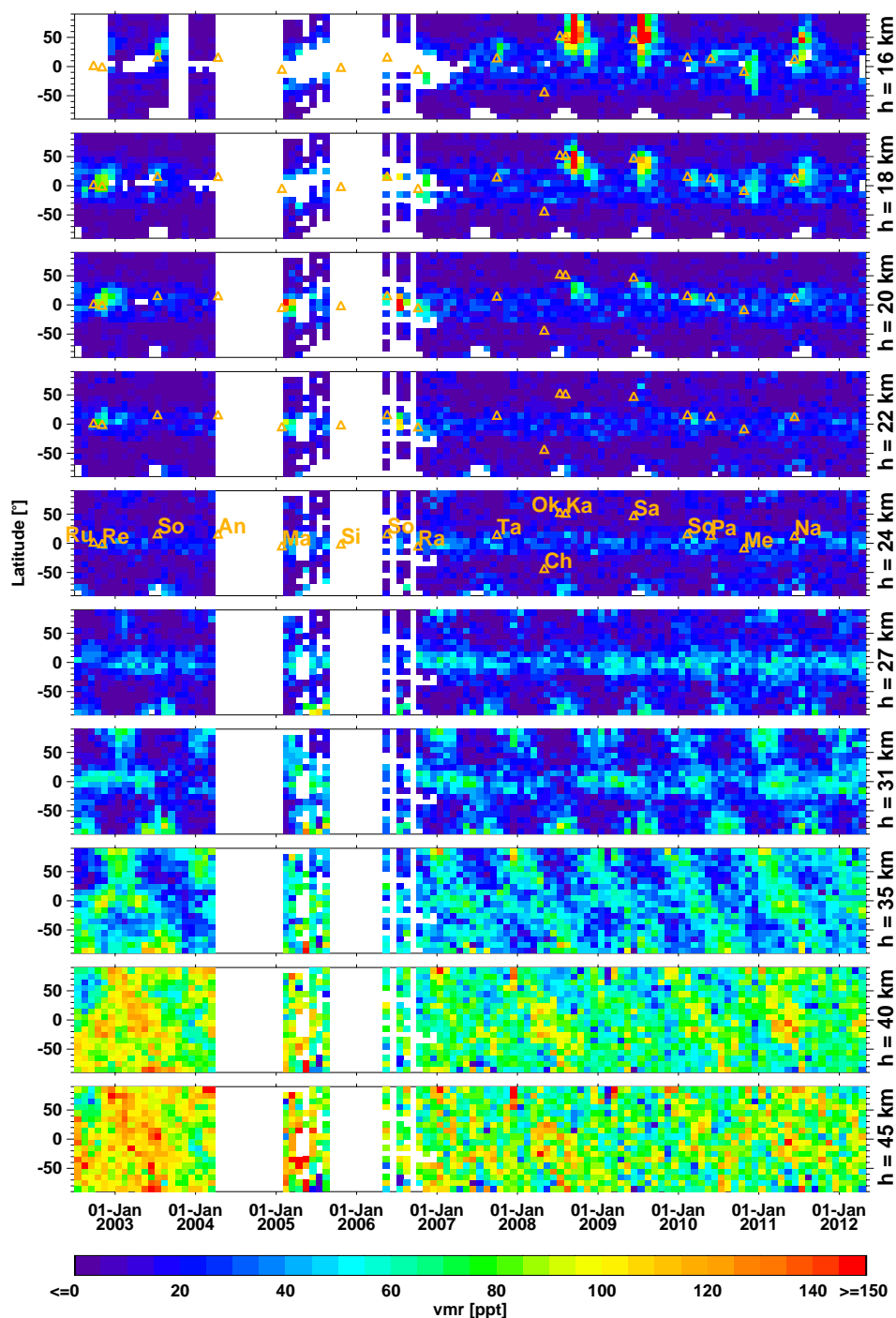


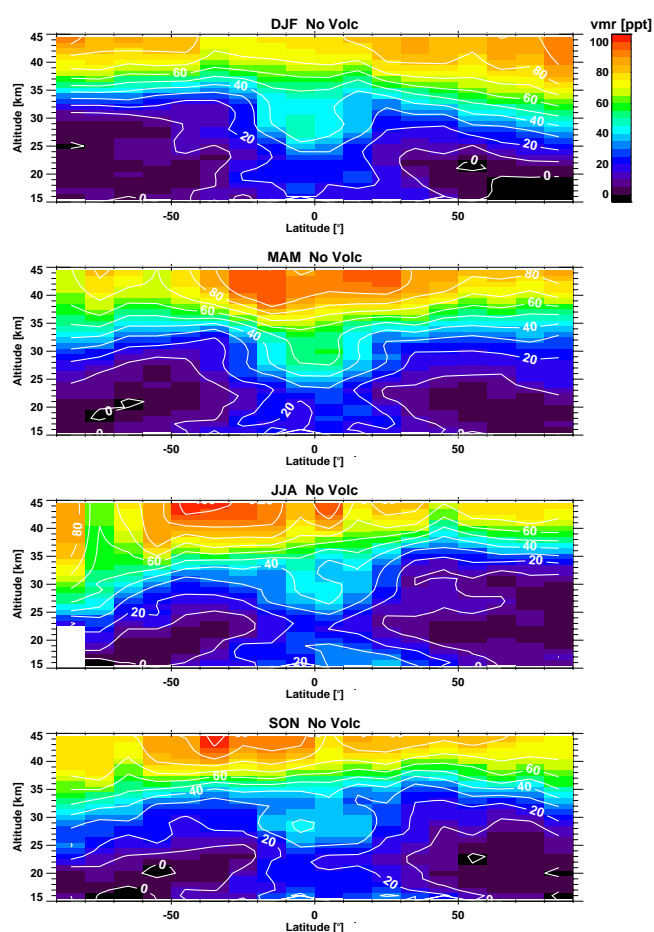
Fig. 6. Global time series of colour-coded SO₂ monthly mean distributions at various altitudes. The colour scale is restricted to 0–150 pptv: negative values and those larger than 150 pptv are given the colour corresponding to 0 and 150 pptv, respectively. Major volcanic eruptions are indicated by the latitude of their location (Table 2).

to values of 400 pptv compared to maximum MIPAS values of 100 pptv. The fact that at lower altitudes around 30 km the values of SO₂ do not deviate from MIPAS as strongly as above 35 km, even for volcanically enhanced conditions,

can most probably be explained with the major part of sulfur being in the form of H₂SO₄ at those altitudes.

Table 1. In situ observations of SO₂ in the lower stratosphere.

Ref.	Date	Location	Altitude [km]	VMR pptv
Jaeschke et al. (1976)	Spring 1976	54° N	14	52
Inn and Vedder (1981)	Jun–Jul 1979	38, 64, 67° N	15.2–20.4	36–51
Meixner (1984)	1978–80	50° N (W-Europe)	10.7–15.2	Dec: 8–33 Apr/May: 13–41(115) Sep: 25–46
Möhler and Arnold (1992)	Feb 1987	67° N (N-Europe)	tropopause tropopause+2.5 km	100 10
Thornton et al. (1999)	1991–1996	W-Pacific	12	60
Jurkat et al. (2010)	Oct 2008	Europe	11.5	20–55 (strat. background) 510 (Kasatochi)

**Fig. 7.** Mean background seasonal distributions of SO₂. Periods of major volcanic influence that have been excluded here are as follows: October–December 2002, July 2003, January–June 2005, May–November 2006, October 2007, July–December 2008, June–December 2009, November–December 2010, July–September 2011.

5.2 Comparison with ACE-FTS

A comparison with observations by ACE-FTS is possible for a volcanically enhanced situation directly after the Sarychev eruption in June 2009. In Fig. 8 of their paper, Doeringer et al. (2012) present the measured zonal median distribution of SO₂ between 12 and 20 km for the first half of July 2009. A direct comparison of the ACE-FTS observations (version 3.0) with those of MIPAS is shown in Fig. 10. For the presentation of the ACE-FTS dataset we have (1) calculated the mean, (2) selected the same latitude bands and (3) performed a linear interpolation to the MIPAS altitude grid. The latitude range 30° N–40° N cannot be used for comparison since there are only two ACE-FTS profiles available, which stem from 1 July and which apparently have not been recorded in volcanically perturbed air masses. Between 40° N and 70° N, both datasets show the enhanced volcanic SO₂ plume with similarly decreasing extension in altitude towards north. Regarding the absolute values, the results from the MIPAS retrievals of SO₂ appear to be generally lower than those of ACE-FTS. In the altitude range 15–19 km the mean difference between the two instruments is 156 pptv ± 68 pptv (54 % ± 19 %). These differences might be due to the locally and temporally sparse coverage of ACE-FTS compared to MIPAS (see the lower panel of Fig. 9 in Doeringer et al. (2012) and number of limb scans used to calculate mean profiles as indicated by orange numbers in Fig. 10). The possibility that the differences are caused by measurement errors of either instrument cannot be excluded. For example, our error estimation for MIPAS retrievals in Fig. 3 indicates relative errors of larger than 100 % in the lowest stratosphere caused by the error term due to analysis from mean spectra. Dedicated simulations of this source of error for volcanically enhanced conditions showed MIPAS results that were 100–150 pptv lower than the real profile at 15–17 km altitude.

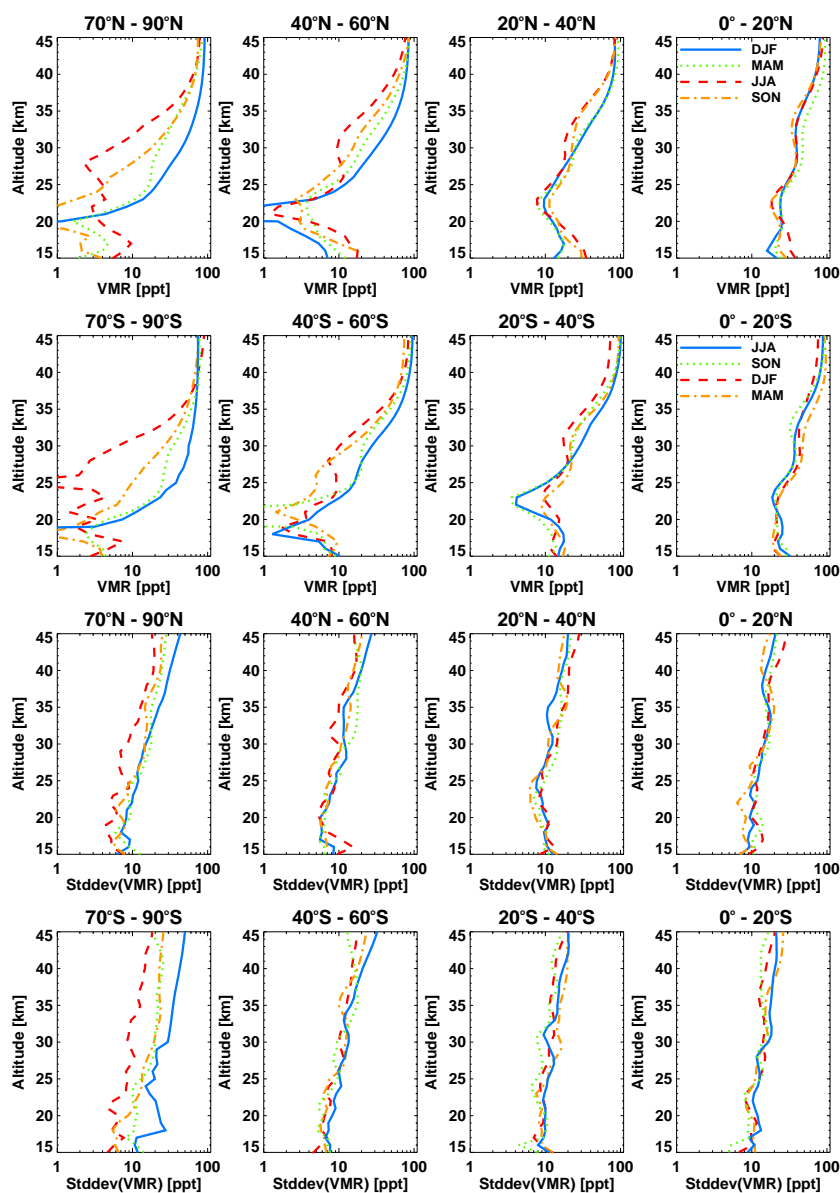


Fig. 8. Mean background seasonal profiles of SO₂ (top two rows) and standard deviation of the distribution (bottom two rows). The legend indicating the seasons in the top row refers to the Northern Hemisphere; the legend in the second row is valid for the Southern Hemisphere. The same periods of major volcanic influence as listed in caption of Fig. 7 have been excluded.

5.3 Comparison with in situ observations

In situ measurements of SO₂ at comparable altitudes to those presented here for the mean MIPAS profiles are extremely sparse since they have mainly been obtained from aircraft up to the lowermost stratosphere. Table 1 shows a selection of published in situ datasets in which explicitly stratospheric values have been indicated that can best be compared to the mean profiles as shown in Fig. 8. The only in situ dataset reaching into the altitude range presented here is the one obtained by Inn and Vedder (1981) up to an altitude of 20.4 km in June/July 1979. The reported values of 36–50 pptv at

15 km are higher (or at the upper end when taking into account the reported error of 50 % of the in situ data) compared to the MIPAS average background vmr distribution (around 13 ± 10 pptv) at mid-latitudes (cf. Fig. 8). At around 20 km, reported SO₂ mixing ratios of 45 and 51 pptv (± 50 %) at 64 and 67° N are clearly much higher than MIPAS mean values, which are around 6 pptv. Even under perturbed situations like the eruption of Sarychev, MIPAS monthly mean data at around 20 km altitude and similar latitudes are less than 20 pptv. Thus, either the aircraft data has been obtained within a locally perturbed situation not representative of the

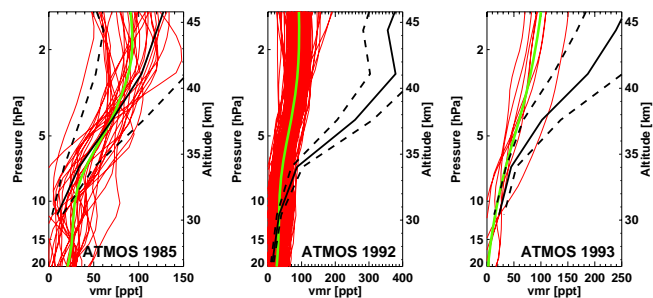


Fig. 9. Comparison of MIPAS observations (2003–2012) of SO₂ (red: single; green: mean) with profiles derived from the ATMOS instrument (black) (Rinsland et al., 1995). Left: SPACELAB 3, April–May 1985, 26° N–32° N vs. MIPAS, April–May 20° N–40° N. Middle: ATLAS 1, March–April 1992, 54° S–28° N vs. MIPAS, March–April 60° S–30° N. Right: ATLAS 2, April 1993, 51° S–44° S vs. MIPAS, April 50° S–40° S.

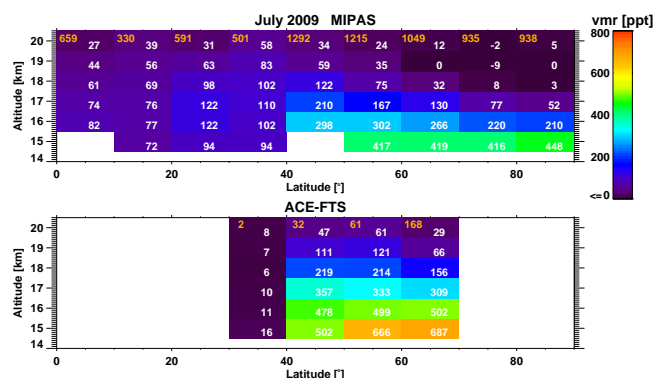


Fig. 10. Latitude–height cross section of MIPAS (top) and ACE-FTS (bottom) zonal mean SO₂ volume mixing ratios in July 2009. Numbers in white show the exact vmr values of each bin in units of ppt. The available number of profiles used to calculate the zonal means are denoted in orange at the top left of each column.

mean background or the difference points to problems of either the in situ data or the MIPAS analysis.

Other observations reaching nearly the lower limit of the altitude range of our MIPAS dataset are the first measurements of SO₂ by Jaeschke et al. (1976) at 14 km and various stratospheric data by Meixner (1984), both obtained in northern mid-latitudes. Comparing the data in Fig. 8 at the lower end of the profiles with those observations shows that MIPAS mean values are generally at the lower part of the variability of the in situ data. However, when considering the generally increasing MIPAS data at northern mid-latitudes with decreasing altitude, it seems reasonable that the typically higher in situ data at lower heights might be compatible. Since the other stratospheric data listed in Table 1 are similar to those already discussed, we conclude that in general the MIPAS values at the bottom end of their altitude range are at the lower limit of in situ observations.

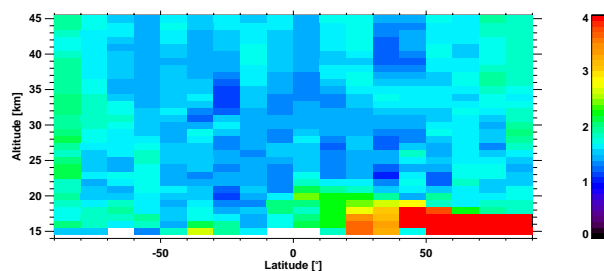


Fig. 11. Global distribution of $\Delta\delta_{l,h}$ as defined in Eq. (3).

5.4 Internal variability

As described in Sect. 3 the instrument noise dominates the error characteristics over a large part of the profile. We have tried to validate this error term by comparing it to the temporal month-to-month variability of the retrieved SO₂ profiles at distinct altitudes for the different latitude bins. This method is similar to the one used for validation of the precision of MIPAS single-scan data products (Piccolo and Dudhia, 2007). Figure 11 shows for each latitude l and altitude h the standard deviation $\Delta\delta_{l,h}$ of the noise-error- ($\epsilon_{l,h,m}$) weighted difference $\delta_{l,h,m}$ of the SO₂ volume mixing ratios $x_{l,h,m}$ between directly subsequent months m in time:

$$\Delta\delta_{l,h} = \left(\frac{1}{M-2} \sum_{m=1}^{M-1} (\delta_{l,h,m} - \bar{\delta}_{l,h})^2 \right)^{\frac{1}{2}} \quad (3)$$

with

$$\delta_{l,h,m} = \frac{x_{l,h,m} - x_{l,h,m+1}}{\sqrt{\epsilon_{l,h,m}^2 + \epsilon_{l,h,m+1}^2}}, \quad (4)$$

where M indicates the number of months and ϵ the estimated error due to instrument spectral noise. In the ideal case $\Delta\delta_{l,h}$ would equal 1. Values greater than 1 indicate either that the natural variability of SO₂ from month to month is not negligible (thus increasing the numerator of Eq. 4) or the noise errors are underestimated (denominator of Eq. 4). In Fig. 11, enhanced values of $\Delta\delta_{l,h}$ in the northern and equatorial lower stratosphere and at all altitudes in high-latitude regions are very likely due to the natural variability caused by volcanic activity and the downwelling of SO₂-rich air into the polar vortices during winter. Anthropogenic influence might be a further source for the enhancements at northern latitudes. Excluding those regions, i.e. for 50° S–50° N and altitudes ≥ 30 km, the mean value of $\Delta\delta_{l,h} = 1.5 \pm 0.1$. Thus, it can be concluded that the estimated noise error may underestimate the instrumental random error by no more than 50%. The difference between estimated noise and month-to-month variability may be explained by either natural variability or by random parts of the total error estimation like variations in the gain calibration or the ECMWF temperature/pressure dataset, which are not included in the pure spectral noise error.

6 Results and discussion

6.1 Mid-stratospheric maximum

The main chemical production of SO₂ in the stratosphere appears via conversion from COS leading to a local maximum of SO₂ in the mid-stratosphere (Crutzen, 1976; Brühl et al., 2012). The MIPAS observations show this maximum to be very pronounced in the tropics, as visible in Figs. 4 and 5, at altitudes of around 27–30 km. The mean latitudinal and seasonal variation of this maximum can better be inspected in averaged stratospheric background profiles as presented in Figs. 7 and 8. For calculation of these profiles major volcanically perturbed seasons (for details see caption of Fig. 7) have been excluded. In the tropics, the mid-stratospheric maximum of the mean profiles is located at 28–30 km, decreasing in altitude towards the poles down to 25 km in the northern and 23 km in the southern summer months. In the tropics, the vmr value of the maximum varies at around 40–50 ppt. Towards higher latitudes, summertime values decrease towards 20 pptv at subtropics, 10 pptv at middle and 5 pptv at polar latitudes. During other seasons the maximum is less discernible from the generally increasing values towards higher altitudes.

The tropical MIPAS values can be compared with model results shown in Fig. 6 of Brühl et al. (2012). Here the altitude of the maximum varies at around 28–31 km, depending on time between 1999 and 2002. In this time range the vmr values vary at around 30–60 pptv, which is similar to the temporal variability of our observations as shown in Figs. 4 and 5.

The local maximum in MIPAS mean profiles of SO₂ (Fig. 8) can further be compared with the results of five different models as shown in SPARC (2006, Fig. 6.11) (<http://www.sparc-climate.org/publications/sparc-reports/sparc-report-no4/>) and Fig. 6.2 of its supplement to Chapter 6. In these simulations the altitude of the tropical maximum is located between 29 and 32 km. The maximum vmr values of 40–50 pptv for four models compare well with MIPAS, while the ULAQ model is considerably lower with about 20 pptv. At 45° latitude in July the models indicate lower maximum altitudes of 24–27 km, in agreement with MIPAS. The model vmr varies here between 8 and 20 pptv, which is comparable to the MIPAS variation between mid-latitude and subtropical mean profile maximum values of 10–20 pptv.

6.2 Enhanced upper stratospheric values and polar downward transport

In the tropics, the production of SO₂ from COS fades out shortly above 30 km due to the unavailability of COS, leading to a decrease of the SO₂ mixing ratio (Brühl et al., 2012). Above about 33 km our measurements show again an increase of SO₂ volume mixing ratios reaching average val-

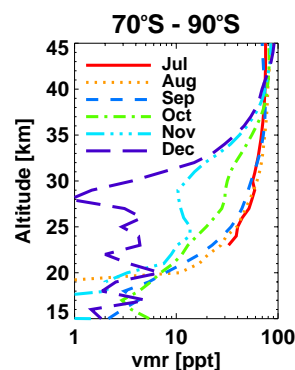


Fig. 12. Temporal evolution of mean Antarctic SO₂ vmr profiles in winter and spring.

ues of about 80–100 pptv (Figs. 8 and 7) at 45 km. At these altitudes, the SO₂ concentrations do not show any large variability with latitude. This increase of SO₂ from the middle to the upper stratosphere is caused by photolysis of H₂SO₄ that is released due to the evaporation of aerosols (Vaida et al., 2003; Mills et al., 2005). At altitudes of 45 km Brühl et al. (2012, Fig. 6) show values of around 50 pptv of SO_x (mostly SO₂), which are considerably smaller than our data. This can be explained by neglecting in the model SO₂ photolysis bands in the visible and near IR (Brühl et al., 2013). The models in SPARC (2006, Fig. 6.11) show large differences at these altitudes: in the tropics three of the models underestimate the observed SO₂ values above the mid-stratospheric maximum, while the LASP model compares rather well. However, at 45° N this model overestimates the high-altitude MIPAS observations by a factor of 2, while other models are still lower than the observations.

In wintertime at high latitudes the MIPAS data show the descent of enhanced upper stratospheric SO₂ concentrations down to 20–25 km altitude (see Fig. 7 and blue curves in Fig. 8). On average, vmr values of 50–60 pptv are reached at 30 km, and 20–40 pptv at 25 km. This periodic effect is clearly visible in the top rows of Figs. 4 and 5. The mean evolution over the Antarctic from July to December is shown in detail in Fig. 12, which can be compared with the simulations shown in Mills et al. (2005, Fig. 5). In those model runs highest SO₂ values of about 100 pptv at 30 km and 60 pptv at 25 km altitude are reached in the Antarctic polar vortex by the end of August. In the observations, highest SO₂ concentrations at these altitudes are observed in July and August with mean values of up to 60 pptv at 30 km and 40 pptv at 25 km altitude (see Fig. 12). In September and October the model shows a sudden decrease of SO₂ concentrations through photolysis leading to the production of small aerosol particles. This behaviour is well reflected in the MIPAS dataset (cf. Fig. 12) where a first decrease is visible below 30 km altitude between August and September, followed by a stronger decrease between September and October below about 35 km.

Table 2. Major volcanic eruptions in the time period of the MIPAS measurements. General data of volcanoes are from <http://www.volcano.si.edu>. Injection heights and SO₂ masses are based on Neely et al. (2013, Table S1) and references therein. References for additional eruptions: Soufrière Hills on 12 July 2003, Carn and Prata (2010); Soufrière Hills on 11 February 2010, Cole et al. (2010); Nabro mass, Clarisse et al. (2012); Nabro injection height, Bourassa et al. (2012) and connected discussion (Fromm et al., 2013; Vernier et al., 2013; Bourassa et al., 2013); Merapi, Suroño et al. (2012). In the case of Pacaya, the SO₂ mass is taken from Aura/OMI measurements on 30 May 2010 (<http://so2.gsfc.nasa.gov>).

Name	Location	Eruption date	SO ₂ mass [Tg]	Injection height [km]
Ruang	2.3° N, 125.4° E	25 Sep 2002	0.055	20
El Reventador	0.1° S, 77.7° W	3 Nov 2002	0.096	17
Soufrière Hills	16.7° N, 62.2° W	12 Jul 2003	0.12	15
Anatahan	16.4° N, 145.7° E	12 Apr 2004	0.065	15
Manam	4.1° S, 145° E	27 Jan 2005	0.18	19
Sierra Negra	0.8° S, 91.2° W	22 Oct 2005	0.36	15
Soufrière Hills	16.7° N, 62.2° W	20 May 2006	0.2	20
Rabaul (Tavurvur)	4.3° S, 152.2° E	7 Oct 2006	0.125	17
Tair, Jebel al	15.5° N, 41.8° E	30 Sep 2007	0.08	16
Chaiten	42.8° S, 72.6° W	2 May 2008	0.01	19
Okmok	53.4° N, 168.1° W	12 Jul 2008	0.122	16
Kasatochi	52.2° N, 175.5° W	7 Aug 2008	1.7	14–18
Sarychev	48.1° N, 153.2° E	12 Jun 2009	1.4	17
Soufrière Hills	16.7° N, 62.2° W	11 Feb 2010	0.05	15
Pacaya	14.4° N, 90.6° W	28 May 2010	0.02	
Merapi	7.5° S, 110.4° E	26 Oct 2010	0.44	17
Nabro	13.4° N, 41.7° E	12 Jun 2011	1.5	14–18

6.3 Lower stratospheric variability

In Fig. 6 we indicated the time and geographical latitude of major volcanic eruptions by orange triangles together with the initials of each volcano as specified in Table 2. As a basis for this list we have taken the one compiled by Neely et al. (2013) and added further eruptions visible in the MIPAS dataset. For that purpose, the retrieval of SO₂ from single MIPAS observations (which is the topic of a separate study to be published) has been used to unambiguously assign elevated amounts of SO₂ to volcanic events. The clear correlation of volcanic eruptions with elevated values of SO₂ in the top four rows of Fig. 6 shows that the major variability of SO₂ in the altitude range below about 22 km is determined by volcanic activity.

In the first half of the MIPAS measurement period, until the end of 2006, equatorial volcanic eruptions dominate the SO₂ mean distribution in the lower stratosphere near the Equator (cf. Figs. 4 and 5), while during the second part mid- and high northern latitudes are mostly affected. Figure 13 compares the temporal evolution of the global SO₂ content derived from MIPAS for the altitude regions 15–23 km and 20–23 km with the total injected mass as derived from nadir-sounding instruments (cf. Table 2). In the case of the larger eruptions of Kasatochi, Sarychev and Nabro, the mean SO₂ content at 15–23 km in the month directly after the eruption is about 1–2 % of the total injected mass. As shown in Sect. 5.2, due to the similar distribution of SO₂ volume mix-

ing ratios between ACE-FTS and MIPAS after the eruption of Sarychev (Doeringer et al., 2012), the total mass derived from both instruments would also be comparable.

For tropical eruptions, like those of Soufrière Hills, El Reventador or Rabaul, the SO₂ mass in the lower stratosphere is of the order of 5 % or more of the total mass, likely due to the general upward transport in the tropical UTLS region. As already indicated in the plots of volume mixing ratio, the lower panel of Fig. 13 shows that altitudes above 20 km are mainly affected by the tropical eruptions before the end of 2006. Roughly about 2 % of the listed total SO₂ mass of tropical volcanoes seems to reach these high altitudes, while this is only about 0.1 % in the case of large mid-latitude eruptions. It should be kept in mind (1) that the MIPAS values of SO₂ mass in 2005 and 2006 are underestimated due to the sparser coverage compared to earlier and later dates, as indicated by the red crosses in Fig. 13, and (2) that due to the cloud threshold described in Sect. 3, strongly aerosol contaminated limb views are excluded from the retrieval leading to a general underestimation of SO₂. The latter effect, however, only affects few limb scans directly after the eruption in the vicinity of the major plume such that the monthly mean values are unlikely to be disturbed.

The SO₂ distributions within the tropical regions in Figs. 4 and 5 can be inspected for indications of upward transport of SO₂ from the periods of volcanically enhanced values in the lower stratosphere up to the SO₂ maximum at around 28 km. After the three major tropical events in the period until 2007

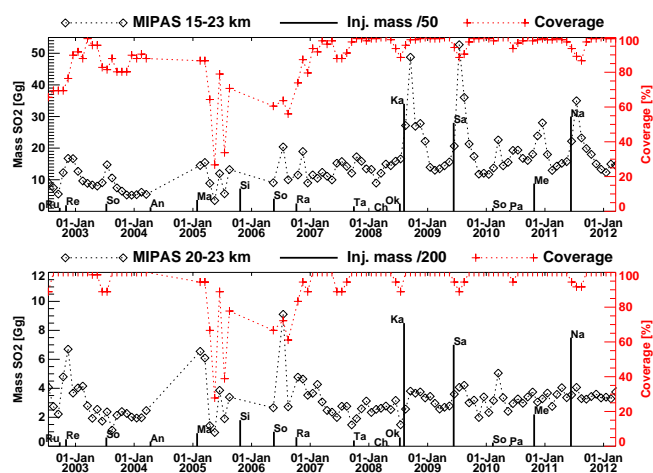


Fig. 13. Black diamonds: global monthly mean SO₂ mass between 15 and 23 km (top) and 20–23 km (bottom) from MIPAS. Black bars: SO₂ injection mass from Table 2 (scaling factor as given in the legend). Red: relative coverage of the latitude–height slice with MIPAS observations.

(end of 2002, beginning of 2005 and mid-2006) an upwelling of SO₂-enhanced air is tentatively visible. However, due to the processing of SO₂ during the months directly after the eruptions, much smaller values of SO₂ remain for an upward transport. It is probable that sulfur is transported in the form of aerosols, as has been shown, for example, in Vernier et al. (2011, Fig. 2). The time series of SO₂ show that enhanced values at its mid-stratospheric maximum near 28 km and above are present some months after the eruptions. However, as described in the following chapter there is a strong correlation with the quasi-biennial oscillation (QBO) especially at those altitudes. The resulting maxima of SO₂ are superposed to possible enhancements due to the volcanic eruptions, and thus both effects are difficult to disentangle.

6.4 Regression analysis

In this section, the temporal development of the SO₂ dataset is analysed under the consideration of a constant term a ; a linear term b ; several periodics; and external parameters with coefficients c , d and e using a multivariate fit approach as proposed by von Clarmann et al. (2010) and extended by Stiller et al. (2012). A regression function $\text{vmr}(t)$ is fitted to the time series of SO₂ values at each 2 km altitude and 10° latitude bin:

$$\begin{aligned} \text{vmr}(t) = & a + bt + c_1\text{qbo}_1(t) + d_1\text{qbo}_2(t) \\ & + c_2 \sin \frac{2\pi t}{T_1} + d_2 \cos \frac{2\pi t}{T_1} \\ & + c_3 \sin \frac{2\pi t}{T_{0.5}} + d_3 \cos \frac{2\pi t}{T_{0.5}} \\ & + eF_{10.7}(t). \end{aligned} \quad (5)$$

Here $\text{qbo}_1(t)$ and $\text{qbo}_2(t)$ are the Singapore time series of winds at 10 hPa and 50 hPa as provided by the Free University of Berlin (<http://www.geo.fu-berlin.de/en/met/ag/strat/produkte/qbo/index.html>). They are used to describe the QBO signal in the time series (Kyrölä et al., 2010). The sine and cosine terms describe annual ($T_1 = 1$ yr) and semi-annual ($T_{0.5} = 0.5$ yr) variability including a phase shift. The solar radio flux at 10.7 cm ($F_{10.7}(t)$) provided by the NOAA Space Weather Prediction Center (<http://www.swpc.noaa.gov>) serves as proxy for solar activity (Kyrölä et al., 2010). A possible offset between P1 and P2 data is accounted for by adding a fully correlated block matrix to the P1 part of the data error covariance matrix.

In Fig. 14, results of the regression analysis are shown for exemplary latitude–height bins illustrating the influence of various partial signals. In the following, Fig. 14 is discussed together with Fig. 15, where the global distribution of the amplitudes of the single regression functions is presented (see caption of Fig. 15 for a more detailed description).

The quality of the fit is illustrated by the χ^2 of the regression (see plot “CHI2” in Fig. 15). In general the global fit quality is relatively homogeneous. The main exceptions are the regions of the polar upper stratosphere and the northern lowermost stratosphere with higher values of χ^2 . The latter is probably explained by volcanic activity the influence of which was mainly concentrated at altitudes up to 20 km in the north (see Sect. 6.3). Further, influences by anthropogenic sources may also contribute to the higher values of χ^2 there. Enhanced χ^2 at high latitudes above 30–35 km altitude stem from strongly increased values of SO₂ up to 120–160 pptv during single winter months (see e.g. top row of Fig. 5), which cannot be represented adequately by the regression model.

The QBO signal can clearly be detected in the tropics at altitudes of 28–36 km introducing a variability in SO₂ of around ± 20 pptv (cf. top right panel in Fig. 15 and example “QBO” in Fig. 14). Here the major part of the QBO signal stems from $\text{qbo}_1(t)$, the Singapore winds at 10 hPa, whereas the winds at 50 hPa ($\text{qbo}_2(t)$) are of minor importance. High values of SO₂ are correlated with the easterly phase of the QBO. Such a QBO signal has also been observed in the case of time series of stratospheric aerosol extinction (Trepte and Hitchman, 1992; Vernier et al., 2011).

Large amplitudes (up to about 30 pptv) of the annual modes are present especially at altitudes of 25–35 km at polar latitudes (cf. Fig. 15). These are explained by the downwelling of SO₂-rich air from higher altitudes during winter. The N–S asymmetry with larger amplitudes at lower altitudes in the south are presumably due to the more persistent Antarctic polar vortex.

The mode of the semi-annual oscillation (SAO) with amplitudes of up to 10 pptv of SO₂ is visible above 30 km altitude at tropical and subtropical latitudes (Fig. 15). This mode can be identified in the example dataset for 20–30° S at 41–43 km altitude (see panel “Semi-annual” in Fig. 14) by

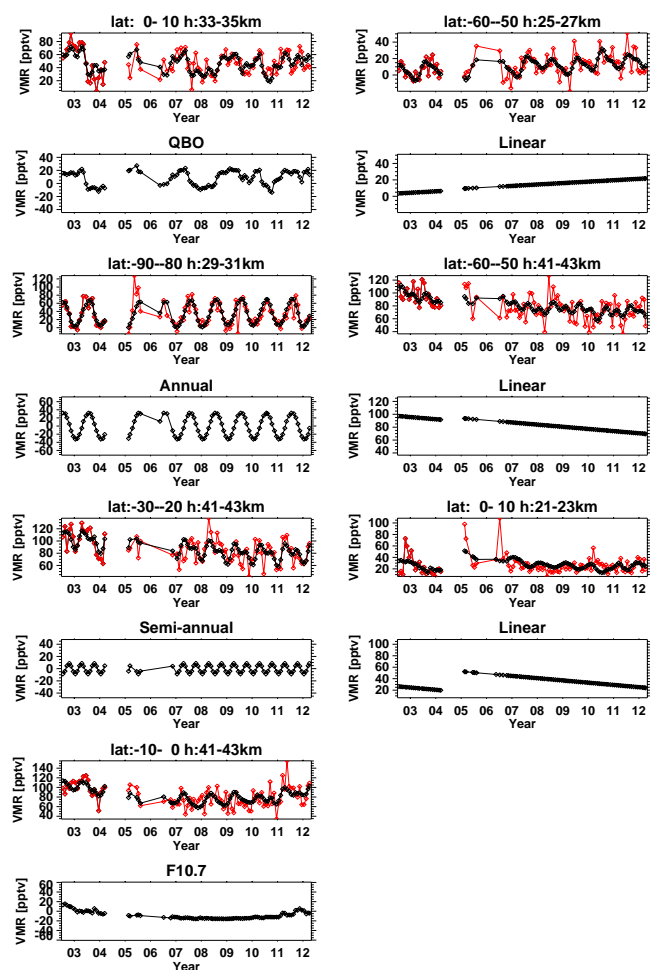


Fig. 14. Time series of multivariate fit results illustrating prominent parameters at different latitude/height regions. Marks along the x axes indicate 1 January of each year. For each parameter, two plots are grouped together: the upper one contains the measured dataset in red and the fit in black for the region as specified in the title; the lower plot illustrates the separate weight of the dedicated parameter listed in the title. Left, rows 1 and 2, linear combination of Singapore winds at 10 and 50 hPa; left, rows 3 and 4, annual variation; left, rows 5 and 6, semi-annual variation; left, rows 7 and 8, solar $F_{10.7}$ flux; right column, linear trend and bias.

a second, smaller peak in the second half of each year. Such a seasonal asymmetry with stronger variation during the first cycle has been described as typical feature of the equatorial SAO (Delisi and Dunkerton, 1988; Garcia et al., 1997). Further, a latitudinal asymmetry of the SAO with stronger intensity southwards of the Equator, as indicated in Fig. 15, has been observed previously in observations of temperature and wind (Belmont and Dartt, 1973; Ray et al., 1998). The global distribution of the reconstructed linear slope is presented in Fig. 15 (bottom right). It shows generally a slight positive trend at all altitudes in the northern and, with larger values, below about 32 km in the southern extra-tropical lat-

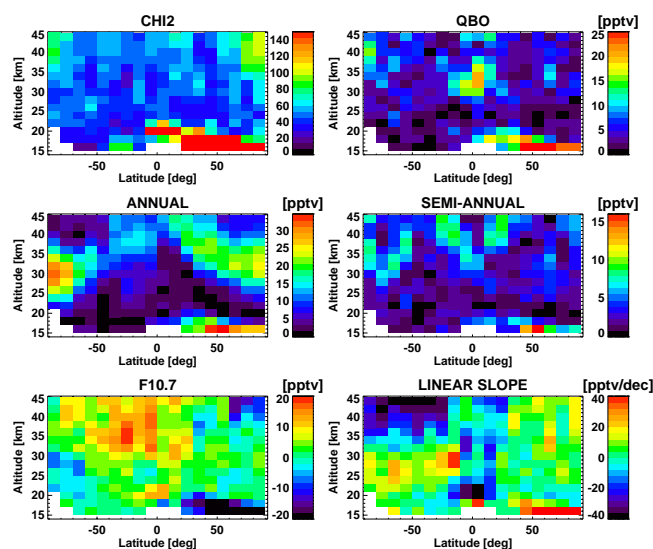


Fig. 15. Global overview of the fit RMS (top left), the amplitudes of various fit parameters and the linear trends (bottom right). For “QBO” and “ $F_{10.7}$ ”, the amplitude is defined as the semi-difference between maximum and minimum of the fitted time series of Singapore winds and solar $F_{10.7}$ flux, respectively. For “ $F_{10.7}$ ” the sign indicates a positive or negative correlation with the solar cycle.

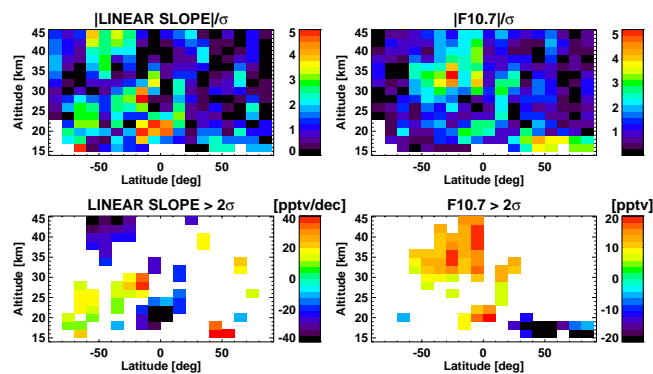


Fig. 16. Top: significance in multiples of the estimated error of the model error corrected linear slope (left) and the $F_{10.7}$ amplitude (see caption of Fig. 15 for definition) (right). Bottom: remaining values with a significance $> 2\sigma$.

itudes. Negative trends are mainly visible at higher altitudes in the southern subtropics and mid-latitudes and at lower altitudes in the tropics. Single examples for time series indicating stronger positive and negative trends at different altitudes in the southern mid-latitudes are shown in Fig. 14. Here at 25–27 km altitude, a positive trend is visible for the whole dataset, and even when considering only data after, for example, 2007. At 41–43 km the data show a general decrease until about 2009 and a levelling-off afterwards. As discussed above, this correlates also with the $F_{10.7}$ flux time series, and it might be that part of the solar variability is mapped into the linear slope (and vice versa). In fact, in Fig. 15 the upper

atmospheric part with negative linear slope in the south is correlated with the area of strongest $F_{10.7}$ amplitude. To determine more specifically the significance of the trend values we have used the method of model-error correction as described in detail in Stiller et al. (2012, Sect. 7). In short, the error covariance matrix of the data is inflated, and mean error correlations are inferred from the fit residuals such as to achieve a unity χ^2 of the fitted trend residuals. This increased error accounts for deficiencies in the linear regression to describe the real atmospheric situation and any underestimation of the measurement errors. The results of this analysis are presented in Fig. 16. The corrected values of the slope are very similar to the ones determined originally under the assumption of measurement error only. The corresponding significance of the slope in terms of its error σ is shown in the middle left of Fig. 16, and in the bottom left part, the remaining data points for which the trend is larger than 2σ are presented. The latter clearly shows that the only larger contiguous area of significant positive trend is located in the Southern Hemisphere reaching from 25 to 30 km in the subtropics down to the lower stratosphere in polar regions. This area separates two regions of negative slope: one above 35 km at austral mid-latitudes, the other in the tropical stratosphere below 25 km. Single time series of the latter (cf. Fig. 14 right, bottom) strongly suggest that the negative slope is caused by larger tropical volcanic influence at the beginning of the first and second MIPAS measurement periods compared to the end of both periods.

A connection with solar activity is indicated by a maximum signal of about 20 pptv for the fit with the $F_{10.7}$ cm flux at mostly tropical and subtropical latitudes above 30–35 km altitude (cf. Fig. 15). This correlation stems from a positive curvature of the 10 yr dataset as visible in panel “ $F_{10.7}$ ” of Fig. 14. It should be kept in mind, however, that there is a correlation between the long-wave $F_{10.7}$ time series, a linear trend and the independent bias values of the first and second MIPAS measurement periods. For example, if SO₂ vmr values of the first period had a systematic positive offset compared to the second period, the $F_{10.7}$ index would partly compensate for it. However, inspection of single time series (like in Fig. 14) reveals that increases after 2010 from a lower constant level during the years 2007–2010 are present in the datasets of the second period, which is in correspondence with the solar cycle. As for the linear trend just described, we have estimated the significance of the solar cycle signal as shown on the right-hand side of Fig. 16. Here the major contiguous area of significant $F_{10.7}$ signal is located in the mid- to upper tropical stratosphere.

7 Conclusions

We have retrieved zonal 10° mean stratospheric distributions of SO₂ from MIPAS/Envisat monthly mean spectra for the period 2002–2012. These are the first observations of ver-

tically resolved SO₂ covering (1) nearly the entire stratosphere, (2) the whole globe and (3) a time period of about 10 yr. Retrieval diagnostics indicate total error bars of 5–20 pptv, most of which is dominated by instrumental noise followed by non-linearity uncertainties due to the retrieval approach at lower altitudes and assumptions on temperature at higher levels. Since the a priori profile of SO₂ has been chosen to be altitude-independent, the shape (apart from some smoothing due to the regularisation type) and the absolute values of the retrieved profiles are entirely based on information from the measurements.

The lack of stratospheric SO₂ observations poses a problem for validation of our dataset. To get an estimate on the data quality, we have performed comparisons with the few available measurements. Above about 30 km there is good consistency with observations from from ATMOS, which provides the only information for this height. To our knowledge, in the altitude range between 20 and 30 km there are no observations of the background SO₂ distribution to compare with. At 14–20 km we could compare with measurements of ACE-FTS during the same volcanically enhanced period showing generally smaller values by MIPAS of around 54 %. This might either be explained by the different temporal and spatial sampling pattern of the two instruments or by measurement errors. A detailed analysis of this issue is envisaged on the basis of MIPAS single-scan retrievals. In situ observations are also sparse above 14 km and not globally available. In general, the MIPAS mid-latitude global mean values at the lower altitudes (about 10–20 pptv with a standard deviation of about 10 pptv) are within, but at the lower limit of, the stratospheric in situ data, with values of roughly 10–50 pptv. Apart from any possible bias of the MIPAS or the in situ datasets this might stem from differences in the observing altitudes (in situ mostly below 15 km) or geographic location for higher altitudes (in situ mostly over northern continents).

A further hint for the validity of our results is the general consistency with the understanding of the behaviour of SO₂ from model results. In this respect we could observe for the first time the local maximum of SO₂ at around 25–30 km resulting from conversion of COS (Brühl et al., 2012). Further, the MIPAS data corroborate the strong increase of SO₂ above 30–35 km, explained by photolysis of H₂SO₄ (Rinsland et al., 1995; Vaida et al., 2003; Mills et al., 2005). The observed increase is larger than the one modelled in Brühl et al. (2012), which can be explained by neglect of the visible and near-IR photolysis bands of H₂SO₄ (Vaida et al., 2003; Brühl et al., 2013). The explanation for the fast increase of small aerosol particles at high latitudes in spring as the conversion from SO₂ on availability of sunlight (Mills et al., 2005) can be followed in terms of an annually reoccurring depletion of SO₂, which has been observed for the first time.

The global, vertically resolved fields of SO₂ in the lower stratosphere over 10 yr confirm the importance of volcanic eruptions for the distribution of sulfate in that region. No

other source of SO₂ comparable to that of volcanoes could be detected. This supports the conclusions of, for example, Neely et al. (2013) and Vernier et al. (2011) on the minor importance of an anthropogenic influence. Further, the current dataset will help to test model simulations on the distribution and total mass entry of SO₂ into the stratosphere based on total SO₂ injection masses from nadir sounders (Neely et al., 2013; Brühl et al., 2013).

A multivariate regression analysis of the SO₂ time series at different altitude–latitude bins with global coverage revealed a QBO signal at around 30 km in the tropics and an SAO signal above at tropical and subtropical latitudes. Further, there appears a possible connection with the solar cycle above 30 km at equatorial and southern mid-latitudes. Significant signals of linear trends are detected at altitudes up to 30 km in the Southern Hemisphere (positive), at high-altitude southern mid-latitudes (negative) and at lower tropical altitudes (negative). The negative linear trend at low latitudes is caused by the signal of tropical volcanic eruptions leading to peaks of enhanced SO₂ volume mixing ratios up until the end of 2006.

In this study we have concentrated on the retrieval from average spectra, which enabled us to get SO₂ distributions throughout the stratosphere with a moderate temporal and latitudinal resolution. These results are, for example, useful for validation of the sulfur budget in chemistry–transport and chemistry–climate models above about 15 km. A direct comparison of such a model with our results is investigated in a parallel study (Brühl et al., 2013). The retrieval from mean spectra is, however, not the optimal way to study the behaviour of SO₂ in the upper troposphere and lowest stratosphere, where a resolution in longitudinal direction and a retrieval down to lower altitudes is desirable. Thus, as a complementary approach, single-profile retrievals from MIPAS, which will cover the altitude range up to about 20 km, are currently in progress. With such a dataset it will, for example, be possible to follow the height-resolved evolution of volcanic plumes.

The retrieval of COS distributions from MIPAS, as investigated initially in Burgess et al. (2005), and the reconstruction of sulfate aerosol properties, as shown in the case of MIPAS-Balloon by Ehle et al. (1998), will be further significant steps forward to reach an experimentally based closure of the stratospheric sulfur budget under conditions of moderate volcanic influence as observed during the lifetime of Envisat.

Supplementary material related to this article is available online at <http://www.atmos-chem-phys.net/13/10405/2013/acp-13-10405-2013-supplement.pdf>.

Acknowledgements. We acknowledge provision of MIPAS level-1b calibrated spectra by ESA, meteorological data by ECMWF, $F_{10.7}$ cm solar radio flux by the NOAA Space Weather Prediction Center, Singapore time series of winds by the Free University of Berlin, and data on volcanic activity by the Smithsonian's

Global Volcanism Program and by NASA's Global Sulfur Dioxide Monitoring Home Page. Funding for the Atmospheric Chemistry Experiment is provided by the Canadian Space Agency. Further we would like to thank Ch. Brühl for helpful discussions. We acknowledge support by the Deutsche Forschungsgemeinschaft and Open Access Publishing Fund of the Karlsruhe Institute of Technology.

The service charges for this open access publication have been covered by a Research Centre of the Helmholtz Association.

Edited by: M. Van Roozendael

References

- Belmont, A. D. and Dartt, D. G.: Semiannual variation in zonal wind from 20 to 65 km at 80° N–10° S, *J. Geophys. Res.*, 78, 6373, doi:10.1029/JC078i027p06373, 1973.
- Bourassa, A. E., Robock, A., Randel, W. J., Deshler, T., Rieger, L. A., Lloyd, N. D., Llewellyn, E. J., and Degenstein, D. A.: Large volcanic aerosol load in the Stratosphere linked to Asian monsoon transport, *Science*, 337, 78–81, doi:10.1126/science.1219371, 2012.
- Bourassa, A. E., Robock, A., Randel, W. J., Deshler, T., Rieger, L. A., Lloyd, N. D., Llewellyn, E. J., and Degenstein, D. A.: Response to Comments on “Large Volcanic Aerosol Load in the Stratosphere Linked to Asian Monsoon Transport”, *Science*, 339, 647, doi:10.1126/science.1227961, 2013.
- Brühl, C., Lelieveld, J., Crutzen, P. J., and Tost, H.: The role of carbonyl sulphide as a source of stratospheric sulphate aerosol and its impact on climate, *Atmos. Chem. Phys.*, 12, 1239–1253, doi:10.5194/acp-12-1239-2012, 2012.
- Brühl, C., Lelieveld, J., Höpfner, M., and Tost, H.: Stratospheric SO₂ and sulphate aerosol, model simulations and satellite observations, *Atmos. Chem. Phys. Discuss.*, 13, 11395–11425, doi:10.5194/acpd-13-11395-2013, 2013.
- Burgess, A. B., Grainger, R. G., and Dudhia, A.: Progress in the retrieval of sulphur species from MIPAS, in: *Envisat ERS Symposium, ESA Special Publication*, vol. 572, 2005.
- Carboni, E., Grainger, R., Walker, J., Dudhia, A., and Sidans, R.: A new scheme for sulphur dioxide retrieval from IASI measurements: application to the Eyjafjallajökull eruption of April and May 2010, *Atmos. Chem. Phys.*, 12, 11417–11434, doi:10.5194/acp-12-11417-2012, 2012.
- Carn, S. A. and Prata, F. J.: Satellite-based constraints on explosive SO₂ release from Soufrière Hills Volcano, Montserrat, *Geophys. Res. Lett.*, 37, L00E22, doi:10.1029/2010GL044971, 2010.
- Clarisse, L., Hurtmans, D., Clerbaux, C., Hadji-Lazaro, J., Ngadi, Y., and Coheur, P.-F.: Retrieval of sulphur dioxide from the infrared atmospheric sounding interferometer (IASI), *Atmos. Meas. Tech.*, 5, 581–594, doi:10.5194/amt-5-581-2012, 2012.
- Cole, P., Bass, V., Christopher, C., Fergus, M., Gunn, L., Odbert, H., Simpson, R., Stewart, R., Stinton, A., Stone, J., Syers, R., Robertson, R., Watts, R., and Williams, P.: Report to the Scientific Advisory Committee on Montserrat Volcanic Activity, Report on Activity between 15 August 2009 and 28 February 2010, Tech. rep., Montserrat Volcano Observatory, open File Report OFR 10-01a, 2010.

- Crutzen, P. J.: The possible importance of CSO for the sulfate layer of the stratosphere, *Geophys. Res. Lett.*, 3, 73–76, doi:10.1029/GL003i002p00073, 1976.
- Delisi, D. P. and Dunkerton, T. J.: Seasonal variation of the semiannual oscillation, *J. Atmos. Sci.*, 45, 2772–2809, doi:10.1175/1520-0469(1988)045<2772:SVOTSO>2.0.CO;2, 1988.
- Deshler, T., Anderson-Sprecher, R., Jäger, H., Barnes, J., Hofmann, D. J., Clemesha, B., Simonich, D., Osborn, M., Grainger, R. G., and Godin-Beekmann, S.: Trends in the nonvolcanic component of stratospheric aerosol over the period 1971–2004, *J. Geophys. Res.*, 111, D01201, doi:10.1029/2005JD006089, 2006.
- Doeringer, D., Eldering, A., Boone, C. D., González Abad, G., and Bernath, P. F.: Observation of sulfate aerosols and SO₂ from the Sarychev volcanic eruption using data from the Atmospheric Chemistry Experiment (ACE), *J. Geophys. Res.*, 117, D03203, doi:10.1029/2011JD016556, 2012.
- Echle, G., von Clarmann, T., and Oelhaf, H.: Optical and microphysical parameters of the Mt. Pinatubo aerosol as determined from MIPAS–B mid–IR limb emission spectra, *J. Geophys. Res.*, 103, 19193–19211, doi:10.1029/98JD01363, 1998.
- Fischer, H., Birk, M., Blom, C., Carli, B., Carlotti, M., von Clarmann, T., Delbouille, L., Dudhia, A., Ehret, D., Endemann, M., Flaud, J. M., Gessner, R., Kleinert, A., Koopman, R., Langen, J., López-Puertas, M., Mosner, P., Nett, H., Oelhaf, H., Perron, G., Remedios, J., Ridolfi, M., Stiller, G., and Zander, R.: MIPAS: an instrument for atmospheric and climate research, *Atmos. Chem. Phys.*, 8, 2151–2188, doi:10.5194/acp-8-2151-2008, 2008.
- Fromm, M., Nedoluha, G., and Charvát, Z.: Comment on “Large Volcanic Aerosol Load in the Stratosphere Linked to Asian Monsoon Transport”, *Science*, 339, 647, doi:10.1126/science.1228605, 2013.
- Garcia, R. R., Dunkerton, T. J., Lieberman, R. S., and Vincent, R. A.: Climatology of the semiannual oscillation of the tropical middle atmosphere, *J. Geophys. Res.*, 102, 26019–26032, doi:10.1029/97JD00207, 1997.
- Hofmann, D., Barnes, J., O’Neill, M., Trudeau, M., and Neely, R.: Increase in background stratospheric aerosol observed with lidar at Mauna Loa Observatory and Boulder, Colorado, *Geophys. Res. Lett.*, 36, L15808, doi:10.1029/2009GL039008, 2009.
- Hofmann, D. J.: Measurement of the condensation nuclei profile to 31 km in the Arctic in January 1989 and comparisons with Antarctic measurements, *Geophys. Res. Lett.*, 17, 357–360, doi:10.1029/GL017i004p00357, 1990.
- Hofmann, D. J. and Rosen, J. M.: Antarctic observations of stratospheric aerosol and high altitude condensation nuclei following the El Chichon eruption, *Geophys. Res. Lett.*, 12, 13–16, doi:10.1029/GL012i001p00013, 1985.
- Höpfner, M., Orphal, J., von Clarmann, T., Stiller, G., and Fischer, H.: Stratospheric BrONO₂ observed by MIPAS, *Atmos. Chem. Phys.*, 9, 1735–1746, doi:10.5194/acp-9-1735-2009, 2009a.
- Höpfner, M., Pitts, M. C., and Poole, L. R.: Comparison between CALIPSO and MIPAS observations of polar stratospheric clouds, *J. Geophys. Res.*, 114, D00H05, doi:10.1029/2009JD012114, 2009b.
- Inn, E. C. Y. and Vedder, J. F.: Measurements of stratospheric sulfur constituents, *Geophys. Res. Lett.*, 8, 5–8, 1981.
- Jaeschke, W., Georgii, H.-W., and Schmitt, R.: Preliminary results of stratospheric SO₂ measurements, *Geophys. Res. Lett.*, 3, 517–519, 1976.
- Jurkat, T., Voigt, C., Arnold, F., Schlager, H., Aufmhoff, H., Schmale, J., Schneider, J., Lichtenstern, M., and Dörnbrack, A.: Airborne stratospheric ITCIMS measurements of SO₂, HCl, and HNO₃ in the aged plume of volcano Kasatochi, *J. Geophys. Res.*, 115, D00L17, doi:10.1029/2010JD013890, 2010.
- Kiefer, M., von Clarmann, T., Grabowski, U., De Laurentis, M., Mantovani, R., Milz, M., and Ridolfi, M.: Characterization of MIPAS elevation pointing, *Atmos. Chem. Phys.*, 7, 1615–1628, doi:10.5194/acp-7-1615-2007, 2007.
- Kyrölä, E., Tamminen, J., Sofieva, V., Bertaux, J. L., Hauchecorne, A., Dalaudier, F., Fussen, D., Vanhellemont, F., Fanton d’Andon, O., Barrot, G., Guirlet, M., Fehr, T., and Saavedra de Miguel, L.: GOMOS O₃, NO₂, and NO₃ observations in 2002–2008, *Atmos. Chem. Phys.*, 10, 7723–7738, doi:10.5194/acp-10-7723-2010, 2010.
- Meixner, F. X.: The vertical sulfur dioxide distribution at the tropopause level, *J. Atmos. Chem.*, 2, 175–189, 1984.
- Mills, M. J., Toon, O. B., and Solomon, S.: A 2D microphysical model of the polar stratospheric CN layer, *Geophys. Res. Lett.*, 26, 1133–1136, doi:10.1029/1999GL000187, 1999.
- Mills, M. J., Toon, O. B., Vaida, V., Hintze, P. E., Kjaergaard, H. G., Schofield, D. P., and Robinson, T. W.: Photolysis of sulfuric acid vapor by visible light as a source of the polar stratospheric CN layer, *J. Geophys. Res.*, 110, D08201, doi:10.1029/2004JD005519, 2005.
- Möhler, O. and Arnold, F.: Gaseous sulfuric acid and sulfur dioxide measurements in the Arctic troposphere and lower stratosphere: implications for hydroxyl radical abundances, *Geophys. Res. Lett.*, 19, 1763–1766, 1992.
- Neely, R. R., Toon, O. B., Solomon, S., Vernier, J. P., Alvarez, C., English, J. M., Rosenlof, K. H., Mills, M. J., Bardeen, C. G., Daniel, J. S., and Thayer, J. P.: Recent anthropogenic increases in SO₂ from Asia have minimal impact on stratospheric aerosol, *Geophys. Res. Lett.*, 40, 999–1004, doi:10.1002/grl.50263, 2013.
- Piccolo, C. and Dudhia, A.: Precision validation of MIPAS-Envisat products, *Atmos. Chem. Phys.*, 7, 1915–1923, doi:10.5194/acp-7-1915-2007, 2007.
- Ray, E. A., Alexander, M. J., and Holton, J. R.: An analysis of the structure and forcing of the equatorial semiannual oscillation in zonal wind, *J. Geophys. Res.*, 103, 1759–1774, doi:10.1029/97JD02679, 1998.
- Read, W. G., Froidevaux, L., and Waters, J. W.: Microwave limb sounder measurement of stratospheric SO₂ from the Mount Pinatubo volcano, *Geophys. Res. Lett.*, 20, 1299–1302, doi:10.1029/93GL00831, 1993.
- Rinsland, C. P., Gunson, M. R., Ko, M. K. W., Weisenstein, D. W., Zander, R., Abrams, M. C., Goldman, A., Sze, N. D., and Yue, G. K.: H₂SO₄ photolysis: a source of sulfur dioxide in the upper stratosphere, *Geophys. Res. Lett.*, 22, 1109–1112, doi:10.1029/95GL00917, 1995.
- Rodgers, C. D.: *Inverse Methods for Atmospheric Sounding: Theory and Practice*, vol. 2, edited by: Taylor, F. W., Series on Atmospheric, Ocean, Planet. Phys., World Scientific, 2000.
- Rosen, J. M. and Hofmann, D. J.: Unusual behavior in the condensation nuclei concentration at 30 km, *J. Geophys. Res.*, 88, 3725–3731, doi:10.1029/JC088iC06p03725, 1983.

- Rothman, L. S., Gordon, I. E., Barbe, A., Benner, D. C., Bernath, P. F., Birk, M., Boudon, V., Brown, L. R., Campargue, A., Champion, J.-P., Chance, K., Coudert, L. H., Dana, V., Devi, V. M., Fally, S., Flaud, J.-M., Gamache, R. R., Goldman, A., Jacquemart, D., Kleiner, I., Lacombe, N., Lafferty, W. J., Mandin, J.-Y., Massie, S. T., Mikhailenko, S. N., Miller, C. E., Moazzen-Ahmadi, N., Naumenko, O. V., Nikitin, A. V., Orphal, J., Perevalov, V. I., Perrin, A., Predoi-Cross, A., Rinsland, C. P., Rotger, M., Šimečková, M., Smith, M. A. H., Sung, K., Tashkun, S. A., Tennyson, J., Toth, R. A., Vandaele, A. C., and Vander Auwera, J.: The HITRAN 2008 molecular spectroscopic database, *J. Quant. Spectrosc. Ra.*, 110, 533–572, doi:10.1016/j.jqsrt.2009.02.013, 2009.
- Solomon, S., Daniel, J. S., Neely, R. R., Vernier, J.-P., Dutton, E. G., and Thomason, L. W.: The persistently variable “Background” stratospheric aerosol layer and global climate change, *Science*, 333, 866–870, doi:10.1126/science.1206027, 2011.
- Spang, R., Remedios, J. J., and Barkley, M. P.: Colour indices for the detection and differentiation of cloud types in infra-red limb emission spectra, *Adv. Space Res.*, 33, 1041–1047, 2004.
- SPARC: Assessment of Stratospheric Aerosol Properties (ASAP), SPARC Report No. 4, WCRP-124, WMO/TD-No. 1295, February 2006, edited by: Thomason, L. and Peter, T., 2006.
- Steck, T.: Methods for determining regularization for atmospheric retrieval problems, *Appl. Opt.*, 41, 1788–1797, 2002.
- Stiller, G. P.: The Karlsruhe Optimized and Precise Radiative Transfer Algorithm (KOPRA), vol. FZKA 6487, Wissenschaftliche Berichte, Forschungszentrum Karlsruhe, 2000.
- Stiller, G. P., von Clarmann, T., Haedel, F., Funke, B., Glatthor, N., Grabowski, U., Kellmann, S., Kiefer, M., Linden, A., Lossow, S., and López-Puertas, M.: Observed temporal evolution of global mean age of stratospheric air for the 2002 to 2010 period, *Atmos. Chem. Phys.*, 12, 3311–3331, doi:10.5194/acp-12-3311-2012, 2012.
- Surono, Jousset, P., Pallister, J., Boichu, M., Buongiorno, M. F., Budisantoso, A., Costa, F., Andreastuti, S., Prata, F., Schneider, D., Clarisse, L., Humaida, H., Sumarti, S., Bignami, C., Griswold, J., Carn, S., Oppenheimer, C., and Lavigne, F.: The 2010 explosive eruption of Java’s Merapi volcano – A “100-year” event, *J. Volcanol. Geoth. Res.*, 241, 121–135, doi:10.1016/j.jvolgeores.2012.06.018, 2012.
- Theys, N., Campion, R., Clarisse, L., Brenot, H., van Gent, J., Dils, B., Corradini, S., Merucci, L., Coheur, P.-F., Van Roozendael, M., Hurtmans, D., Clerbaux, C., Tait, S., and Ferrucci, F.: Volcanic SO₂ fluxes derived from satellite data: a survey using OMI, GOME-2, IASI and MODIS, *Atmos. Chem. Phys. Discuss.*, 12, 31349–31412, doi:10.5194/acpd-12-31349-2012, 2012.
- Thornton, D. C., Bandy, A. R., Blomquist, B. W., Driedger, A. R., and Wade, T. P.: Sulfur dioxide distribution over the Pacific Ocean 1991–1996, *J. Geophys. Res.*, 104, 5845–5854, 1999.
- Tikhonov, A.: On the solution of incorrectly stated problems and method of regularization, *Dokl. Akad. Nauk. SSSR*, 151, 501–504, 1963.
- Trepte, C. R. and Hitchman, M. H.: Tropical stratospheric circulation deduced from satellite aerosol data, *Nature*, 355, 626–628, doi:10.1038/355626a0, 1992.
- Vaida, V., Kjaergaard, H. G., Hintze, P. E., and Donaldson, D. J.: Photolysis of sulfuric acid vapor by visible solar radiation, *Science*, 299, 1566–1568, doi:10.1126/science.1079297, 2003.
- Van Gent, J., Spurr, R., Lerot, C., Van Roozendael, M., Theys, N., and Brenot, H.: SO₂ plume height retrieval from direct fitting of GOME-2 backscattered radiance measurements, in: 39th COSPAR Scientific Assembly, 14–22 July 2012, Mysore, India, Abstract C0.3-1-12, p.2048, vol. 39, COSPAR Meeting, 2012.
- Vernier, J.-P., Thomason, L. W., Pommereau, J.-P., Bourassa, A., Pelon, J., Garnier, A., Hauchecorne, A., Blanot, L., Trepte, C., Degenstein, D., and Vargas, F.: Major influence of tropical volcanic eruptions on the stratospheric aerosol layer during the last decade, *Geophys. Res. Lett.*, 38, L12807, doi:10.1029/2011GL047563, 2011.
- Vernier, J.-P., Thomason, L. W., Fairlie, T. D., Minnis, P., Palikonda, R., and Bedka, K. M.: Comment on “Large Volcanic Aerosol Load in the Stratosphere Linked to Asian Monsoon Transport”, *Science*, 339, 647, doi:10.1126/science.1227817, 2013.
- von Clarmann, T., Ceccherini, S., Doicu, A., Dudhia, A., Funke, B., Grabowski, U., Hilgers, S., Jay, V., Linden, A., López-Puertas, M., Martín-Torres, F.-J., Payne, V., Reburn, J., Ridolfi, M., Schreier, F., Schwarz, G., Siddans, R., and Steck, T.: A blind test retrieval experiment for infrared limb emission spectrometry, *J. Geophys. Res.*, 108, 4746, doi:10.1029/2003JD003835, 2003a.
- von Clarmann, T., Glatthor, N., Grabowski, U., Höpfner, M., Kellmann, S., Kiefer, M., Linden, A., Mengistu Tsidu, G., Milz, M., Steck, T., Stiller, G. P., Wang, D. Y., Fischer, H., Funke, B., Gil-López, S., and López-Puertas, M.: Retrieval of temperature and tangent altitude pointing from limb emission spectra recorded from space by the Michelson Interferometer for Passive Atmospheric Sounding (MIPAS), *J. Geophys. Res.*, 108, 4736, doi:10.1029/2003JD003602, 2003b.
- von Clarmann, T., Höpfner, M., Kellmann, S., Linden, A., Chauhan, S., Funke, B., Grabowski, U., Glatthor, N., Kiefer, M., Schieferdecker, T., Stiller, G. P., and Versick, S.: Retrieval of temperature, H₂O, O₃, HNO₃, CH₄, N₂O, ClONO₂ and ClO from MIPAS reduced resolution nominal mode limb emission measurements, *Atmos. Meas. Tech.*, 2, 159–175, doi:10.5194/amt-2-159-2009, 2009.
- von Clarmann, T., Stiller, G., Grabowski, U., Eckert, E., and Orphal, J.: Technical Note: Trend estimation from irregularly sampled, correlated data, *Atmos. Chem. Phys.*, 10, 6737–6747, doi:10.5194/acp-10-6737-2010, 2010.
- Wilson, J. C., Stolzenburg, M. R., Clark, W. E., Loewenstein, M., Ferry, G. V., and Chan, K. R.: Measurements of condensation nuclei in the airborne arctic stratospheric expedition – observations of particle production in the polar vortex, *Geophys. Res. Lett.*, 17, 361–364, doi:10.1029/GL017i004p00361, 1990.
- Zhao, J., Toon, O. B., and Turco, R. P.: Origin of condensation nuclei in the springtime polar stratosphere, *J. Geophys. Res.*, 100, 5215–5227, doi:10.1029/94JD03110, 1995.